CrystEngComm

PAPER

View Article Online
View Journal | View Issue

Cite this: *CrystEngComm*, 2023, **25**, 3922

Synthesis, structure diversity, and antimicrobial studies of Ag(I) complexes with quinoline-type ligands†

Amal Yousri,[a] Matti Haukka,[b] Morsy A. M. Abu-Youssef,*[a] Mohammed Salah Ayoup,*[a] Magda M. F. Ismail,[c] Nagwan G. El Menofy,[d] Saied M. Soliman,[a] Assem Barakat,[e] Francoise M. Amombo Noa[f] and Lars Öhrström*[f]

Compounds [Ag(**5NO$_2$Qu**)$_2$]BF$_4$ (**1**) and [Ag(**Qu3CN**)(H$_2$O)]BF$_4$ (**2**) were prepared and studied from a structural perspective and screened for antimicrobial activity. The Ag(I) in the monomeric complex **1** is coordinated to two 5-nitroquinoline (**5NO$_2$Qu**) ligands *via* the N-atoms of the quinoline rings with equidistant Ag–N bonds (2.146(2) Å) and a N–Ag–N$^{\#}$ bond angle of 171.42(8)°. The 2D coordination polymer **2** contains tetracoordinated Ag(I) with two N-atoms (N1 and N2$^{\#1}$) from two quinoline-3-carbonitrile (**Qu3CN**) ligands and two O-atoms (O1 and O1$^{\#1}$) from two water molecules. The **Qu3CN** ligand acts as a connector between the Ag(I) sites along the *b*-direction *via* two short Ag1–N1 (2.185(4) Å) and Ag1–N2$^{\#1}$ (2.204(4) Å) bonds. In addition, the Ag(I) is coordinated with two symmetry related water molecules which are also acting as connectors between the Ag(I) sites along the *a*-direction *via* two longer Ag1–O1 (2.470(4) Å) and Ag1–O1$^{\#2}$ (2.546(4) Å) bonds. Hirshfeld surface analysis confirmed the significance of the polar F···H contacts in the molecular packing of **1** (25.9%) and **2** (39.9%). In addition, the crystal packing of **1** showed a significant amount of polar O···H (23.5%) contacts. Also, both complexes displayed π–π stacking interactions. The Ag(I) complexes and the free ligand were assessed for their antimicrobial activities. It was found that **1** (MIC = 7.8 μg mL^{-1}) and **2** (MIC = 31.25 μg mL^{-1}) have higher antifungal potency against *C. albicans* than their free ligands (MIC = 125 μg mL^{-1}). Interestingly, **1** has better antifungal activity than the standard nystatin (15.6 μg mL^{-1}). Also, both Ag(I) complexes and the free ligands as well have better activity against *P. mirabilis* than the common antibiotic amoxicillin.

Received 24th April 2023,
Accepted 15th June 2023

DOI: 10.1039/d3ce00417a

rsc.li/crystengcomm

1. Introduction

The use of transition metal compounds as therapeutic agents has attracted the attention of researchers for a long time.[1–6] The reason is that coordination compounds may be effective in drug design, particularly for the creation of innovative antimicrobial drugs, due to the enormous variety of metals, ligands, and geometries.[7] Over a long period of time, considerable interest has been shown in Ag(I) and its complexes. Due to the d^{10}-electron configuration of Ag(I), it forms a wide range of geometries as it lacks stereochemical selectivity, except some preference for linear two-coordinated complexes.

The coordination geometry of Ag(I) complexes can thus be linear,[8–11] trigonal planar,[12–14] T-shaped,[15,16] square planar,[17,18] tetrahedral,[19,20] trigonal bipyramidal,[21,22] square pyramidal,[23,24] and octahedral.[25–27]

These complexes show a wide range of biological activities against bacteria, fungi, viruses, and cancerous cells.[28–32] Also, Ag(I) and its complexes have potential uses in wound treatment and can be used in anti-infection creams.[33–35]

On the other hand, quinoline and its derivatives represent a significant category of nitrogen heterocycles[36,37] which have interesting structural characteristics capable of influencing the geometry of their metal complexes.

[a] *Department of Chemistry, Faculty of Science, Alexandria University, P.O. Box 426, Ibrahimia, Alexandria 21321, Egypt. E-mail: morsy5@alexu.edu.eg, saied1soliman@yahoo.com*
[b] *Department of Chemistry, University of Jyväskylä, P.O. Box 35, FI-40014 Jyväskylä, Finland. E-mail: matti.o.haukka@jyu.fi*
[c] *Department of Pharmaceutical Medicinal Chemistry, Faculty of Pharmacy (Girls), Al-Azhar University, Cairo, Egypt*
[d] *Department of Microbiology and Immunology, Faculty of Pharmacy (Girls), Al-Azhar University, Cairo, Egypt. E-mail: m.elalfy101@gmail.com*
[e] *Department of Chemistry, College of Science, King Saud University, P.O. Box 2455, Riyadh 11451, Saudi Arabia. E-mail: ambarakat@ksu.edu.sa*
[f] *Chemistry and Biochemistry, Dept. of Chemistry and Chemical Engineering, Chalmers University of Technology, SE-41296 Göteborg, Sweden. E-mail: mystere@chalmers.se, ohrstrom@chalmers.se*

† Electronic supplementary information (ESI) available. CCDC 2246560 and 2246561. For ESI and crystallographic data in CIF or other electronic format see DOI: https://doi.org/10.1039/d3ce00417a

The main reason for such structural properties is the existence of π–π stacking which is one of the significant non-covalent interactions between the atoms of fused polycyclic aromatic rings.[38] Also, quinoline based derivatives are considered structural components of many medicines with antibacterial, antimalarial, and anticancer properties.[36–46] Generally, quinolines are commonly used in many aspects such as the production of herbicides, corrosion inhibitors, and sensors.[36,47] In addition, aromatic compounds with nitro groups, especially nitroquinoline derivatives, are frequently used in the manufacture of drugs, dyes, and explosives.[48]

Recently, combinations of N-heterocycles with Ag(I) ions to produce more effective antibacterial agents have been reported.[49–52] Quinoline-type ligands are one of the most prominent N-heterocycles which form Ag(I) complexes with versatile structures and interesting biological activity.[38] In this work, two new Ag(I) complexes with the 5-nitroquinoline (**5NO$_2$Qu**) and quinoline-3-carbonitrile (**Qu3CN**) ligands were synthesized (Fig. 1). The Ag(I) complexes were characterized using several experimental methods including elemental analysis, FTIR, NMR and single crystal X-ray diffraction combined with Hirshfeld calculations. In the light of the remarkable antimicrobial activity of Ag(I) complexes and quinolines as well, the antimicrobial activities of the newly synthesized Ag(I) complexes were assessed.

2. Experimental

2.1 Materials and methods

2.1.1 Materials and physical measurements. All materials used, including solvents and chemicals, were of analytical grade and purchased from Sigma-Aldrich Company. A Perkin Elmer 2400 elemental analyzer (Inc.940 Winter Street, Waltham, MA, USA) was used for CHN elemental analysis. The Ag content was determined using a Shimadzu atomic absorption spectrophotometer (AA-7000 series, Shimadzu, Ltd., Japan). FTIR analysis was performed in KBr pellets using a Bruker Tensor 37 FTIR instrument (Waltham, MA, USA) in the range 4000–400 cm^{-1} and a JEOL-400 MHz spectrometer was used for NMR spectra collection in DMSO-d_6.

2.1.2 Synthesis. The two target Ag(I) complexes were synthesized by mixing the functional ligand (**5NO$_2$Qu** or **Qu3CN**) in ethanol with an aqueous $AgBF_4$ solution, and then acetonitrile was added to dissolve the resulting turbidity. The clear solution was left to slowly evaporate at room temperature. Complexes **1** and **2** were formed as colorless crystals after five days and then collected from solution by filtration. The resulting crystals were found suitable for X-ray single crystal structure analysis.

*[Ag(**5NO$_2$Qu**)$_2$]BF$_4$ (**1**).* $AgBF_4$ (77.9 mg, 0.4 mmol) in 5 mL distilled water was mixed with **5NO$_2$Qu** (139.3 mg, 0.8 mmol) in 10 mL ethanol giving a turbid solution. Acetonitrile was added dropwise until the solution became clear. The clear solution was left to slowly evaporate at room temperature giving colorless crystals after five days which were collected from solution by filtration. Yield: 85%; anal. calc. $C_{18}H_{12}AgBF_4N_4O_4$: C, 39.82; H, 2.23; N, 10.32; Ag, 19.87%. Found: C, 39.60; H, 2.15; N, 10.31; Ag, 19.69%. FTIR cm^{-1}: 3105, 3072, 1624, 1592, 1521, 1341, 1066, 1031. Ligand (**5NO$_2$Qu**): 3071, 1626, 1593, 1520, 1321 (Fig. S1†). ^{1}H NMR (500 MHz, DMSO-d_6), δ_H: 9.04 (dd, J = 4.0 Hz, 1.5 Hz, 1H, Ar–H), 8.79 (d, J = 8.5 Hz, 1H, Ar–H), 8.40 (t, J = 8.5 Hz, 2H, Ar–H), 7.92 (t, J = 8.0 Hz, 1H, Ar–H), 7.76 (dd, J = 8.0 Hz, 4.5 Hz, 1H, Ar–H); ^{13}C NMR (125 MHz, DMSO-d_6) δ_C: 152.5, 147.9, 145.8, 136.5, 131.9, 128.9, 125.2, 124.8, 120.7 (Fig. S2†). [Ag(**5NO$_2$Qu**)$_2$]BF$_4$ (**1**): ^{1}H NMR (500 MHz, DMSO-d_6), δ_H: 9.05 (dd, J = 4.0 Hz, 4.0 Hz, 1H, Ar–H), 8.81 (d, J = 8.5 Hz, 1H, Ar–H), 8.42 (t, J = 8.5 Hz, 2H, Ar–H), 7.93 (t, J = 8.0 Hz, 1H, Ar–H), 7.78 (dd, J = 8.5 Hz, 4.5 Hz, 1H, Ar–H); ^{13}C NMR (125 MHz, DMSO-d_6) δ_C: 152.7, 147.9, 145.9, 136.5, 132.1, 128.9, 125.4, 124.7, 120.7 (Fig. S3†).

*[Ag(**Qu3CN**)(H$_2$O)]BF$_4$ (**2**).* $AgBF_4$ (77.9 mg, 0.4 mmol) in 5 mL distilled water was mixed with **Qu3CN** (61.7 mg, 0.4 mmol) in 5 mL ethanol giving a turbid solution. Acetonitrile was added dropwise until the solution became clear. The clear solution was left to slowly evaporate at room temperature giving colorless crystals after five days which were collected from solution by filtration. Yield: 88%; anal. calc. $C_{10}H_8AgBF_4N_2O$: C, 32.74; H, 2.20; N, 7.64; Ag, 29.40%. Found: C, 32.55; H, 2.13; N, 7.51; Ag, 29.25%. FTIR cm^{-1}: 3354, 3062, 2227, 1621, 1567, 1063, 1033. Ligand (**Qu3CN**): 3060, 2226, 1618, 1565 (Fig. S4†). ^{1}H NMR (500 MHz, DMSO-d_6), δ_H: 9.13 (d, J = 1.5 Hz, 1H, Ar–H), 9.05 (d, J = 2.5 Hz, 1H, Ar–H), 8.08 (t, J = 9.0 Hz, 2H, Ar–H), 7.94 (t, J = 8.5 Hz, 1H, Ar–H), 7.74 (t, J = 8.0 Hz, 1H, Ar–H); ^{13}C NMR (125 MHz, DMSO-d_6) δ_C: 150.7, 148.5, 143.0, 133.5, 129.5, 129.9, 128.9, 126.4, 117.9 (Ar–C), 106.3 (CN) (Fig. S5†). [Ag(**Qu3CN**)(H$_2$O)]BF$_4$ (**2**): ^{1}H NMR (500 MHz, DMSO-d_6), δ_H: 9.13 (d, J = 2.5 Hz, 1H, Ar–H), 9.06 (d, J = 1.5 Hz, 1H, Ar–H), 8.08 (t, J = 9.0 Hz, 2H, Ar–H), 7.95 (t, J = 8.5 Hz, 1H, Ar–H), 7.75 (t, J = 7.5 Hz, 1H, Ar–H); ^{13}C NMR (125 MHz, DMSO-d_6) δ_C: 150.6, 148.5, 143.1, 133.6, 129.6, 129.4, 128.9, 126.4, 118.0 (Ar–C), 106.3 (CN) (Fig. S6†).

2.1.3 Crystallographic measurements. The crystal structures of **1** and **2** were determined using the procedures described in the ESI† (Method S1).[53–56] The crystallographic details are summarized in Table 1. The crystallographic data and details of the structure refinements are given in Table 1. CCDC 2246560 and CCDC 2246561 contain the crystallographic data for [Ag(**5NO$_2$Qu**)$_2$]BF$_4$ (**1**) and for [Ag(**Qu3CN**)(H$_2$O)]BF$_4$ (**2**) respectively.

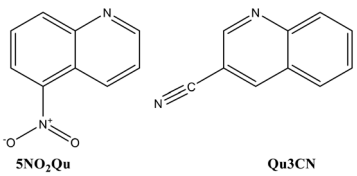

Fig. 1 5-Nitroquinoline (**5NO$_2$Qu**) and quinoline-3-carbonitrile (**Qu3CN**).

Table 1 Crystallographic parameters for $[Ag(\mathbf{5NO_2Qu})_2]BF_4$ (**1**) and $[Ag(\mathbf{Qu3CN})(H_2O)]BF_4$ (**2**)

Complex number	**1**	**2**
Empirical formula	$C_{18}H_{12}AgBF_4N_4O_4$	$C_{10}H_8AgBF_4N_2O$
Formula weight (g mol^{-1})	543	366.86
Temperature	170(2) K	120(2) K
Wavelength	0.71073 Å	1.54184 Å
Crystal system	Monoclinic	Monoclinic
Space group	*C*2/*c*	*C*2/*c*
Unit cell dimensions	a = 9.8173(4) Å	a = 10.0480(2) Å
	b = 12.9566(6) Å	b = 16.8535(2) Å
	c = 14.7156(4) Å	c = 14.5843(2) Å
	β = 101.124(2)°	β = 98.505(2)°
Volume	1836.64(12) Å^3	2442.60(7) Å^3
Z	4	8
Density (calc.)	1.964 Mg m^{-3}	1.995 Mg m^{-3}
Abs. coefficient	1.175 mm^{-1}	13.686 mm^{-1}
F(000)	1072	1424
Crystal size (mm)	0.237 × 0.202 × 0.122	0.095 × 0.040 × 0.018
Theta range	2.635 to 29.699°	5.167 to 77.338°
Index ranges	$-13 \le h \le 13$, $-16 \le k \le 17$, $-20 \le l \le 20$	$-12 \le h \le 11$, $-21 \le k \le 21$, $-18 \le l \le 18$
Reflections	14 574	45 689
Indep. reflections	2566 [R(int) = 0.0265]	2596 [R(int) = 0.0851]
Completeness	99.30%	100.00%
Absorption correction	Semi-empirical from equivalents	Gaussian
Max. and min. transm.	0.7459 and 0.6792	1.000 and 0.928
Refinement method	Full-matrix least-squares on F^2	Full-matrix least-squares on F^2
CCDC	CCDC 2246560	CCDC 2246561

2.2 Hirshfeld surface analysis

Hirshfeld surfaces and 2D fingerprint plots[55] were calculated using Crystal Explorer 17.5 software.[56]

2.3 Antimicrobial studies

The antimicrobial activity of complexes **1** and **2** as well as the free ligands was screened against some harmful microbes as described in Method S1 (ESI†).[57]

3. Results and discussion

3.1 Chemistry and characterization

The two target Ag(I) complexes were synthesized using the self-assembly technique by mixing the functional ligand (**5NO$_2$Qu** or **Qu3CN**) in ethanol with an aqueous $AgBF_4$ solution, and then acetonitrile was added to dissolve the resulting turbidity (Scheme 1). The clear solution was left to slowly evaporate at room temperature. Complexes **1** and **2** were obtained as colourless crystals after five days, which were found suitable for the X-ray single crystal structure analysis.

Their structures were confirmed using FTIR, ^{1}H-NMR, and ^{13}C-NMR. The FTIR spectra of the synthesized complexes compared to those of the corresponding free ligands are presented in Fig. S1 and S2.† The FTIR spectra of complexes **1** and **2** showed expected peaks of the free ligands with some deviations. Symmetric and asymmetric N–O stretches were detected at 1520 and 1321 cm^{-1} in the free **5NO$_2$Qu** while in complex **1**, the corresponding values are 1521 and 1341 cm^{-1}.[58] In the case of **5NO$_2$Qu**, the $\nu_{(C=N)}$ and $\nu_{(C=C)}$ stretching modes appeared at 1626 and 1593 cm^{-1}, respectively, while these appeared at 1618 and 1565 cm^{-1} for **Qu3CN**. On the other hand, the $\nu_{(C=N)}$ and $\nu_{(C=C)}$ modes appeared at 1624 and 1592 cm^{-1}, respectively, in **1** while for complex **2**, the corresponding values are 1621 and 1567 cm^{-1}. In addition, the peak that appeared at 2227 cm^{-1} in the free **Qu3CN** and **2** could be assigned to the $\nu_{(C=N)}$ mode. Also, complex **2** showed the characteristic $\nu_{(O-H)}$ mode of coordinated water molecules at 3354 cm^{-1}. In both complexes, the characteristic stretching vibrations of BF_4^- were detected as broad double split peaks at 1066 and 1031 cm^{-1} for complex **1**, and at 1063 and 1033 cm^{-1}

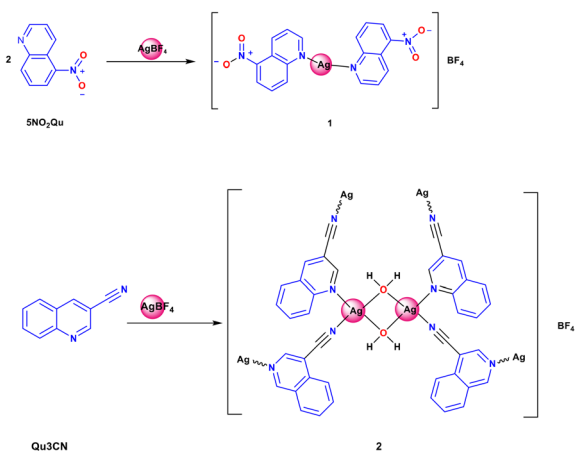

Scheme 1 Synthesis of complexes **1** and **2**.

for complex **2**. These peaks are completely absent in the FTIR spectra of the free ligands which sheds light on the possible coordination between Ag(I) and the quinoline ligands in both complexes.

In addition, the ^{1}H NMR and ^{13}C NMR spectra (see the ESI†) of both complexes showed a characteristic small shift in the signals compared to those of the free ligands which might be evidence for the presence of coordinated ligands in solution[38,59,60] However, the exact nature and mix of Ag(I) species in solution remain elusive. Typically these complexes have fast ligand exchange on the NMR scale and the equilibrium may favour substantial proportions of free ligands under stoichiometric conditions, hence the small NMR shift changes and also the noticeably smaller shift changes for **2** that has half the ligand/Ag ratio compared to **1**. However, the different species in solution will also have different biological potencies and it is not unlikely that minor species have higher antibacterial activity.[38,60]

This behaviour is generally known for silver(I) complexes with N-donor ligands, which may have relatively weak Ag–N and Ag–O interactions, although this depends on the exact nature of the nitrogen (*i.e.* NH_3 is different from pyridine).[59] Silver(I) complexes with high stability in biological fluids are undesirable for biological applications. In contrast, those with weak Ag–ligand (Ag–N and Ag–O) bonds which have high ability for ligand replacement by biomolecules inside the body are powerful antimicrobial agents.[61–64]

3.2 Single crystal X-ray structures

3.2.1 [Ag(5NO2Qu)$_2$]BF$_4$, 1. [Ag(**5NO2Qu**)$_2$]BF$_4$, **1**, crystallized in the monoclinic crystal system with the *C*2/*c* space group (see Table 1). The asymmetric unit contains one half [Ag(**5NO2Qu**)$_2$]BF$_4$ due to the presence of a molecular two-fold rotational axis. A representation of the structure of this monomeric complex is shown in Fig. 2.

In the cationic inner sphere [Ag(**5NO$_2$Qu**)$_2$]$^+$, the Ag(I) is coordinated to two symmetry related **5NO$_2$Qu** molecules *via* the quinoline N-atom as a monodentate ligand. The two **5NO$_2$Qu** molecules are *anti* to one another possibly to minimize the steric hindrance between the two bulky quinoline moieties. The two-symmetry related Ag1–N1 and Ag1–N1$^{\#}$ bonds are equidistant (2.146(2) Å). The N1–Ag1–N1$^{\#}$ angle (171.42(8)°) deviates slightly from the ideal value of 180° possibly due to steric hindrance between the two ligands (H8···H1 distance: 3.540(7) Å) or interactions with the counterions. Another possibility is Ag···O interactions (see Fig. 3), as both O1···Ag1 at 3.073(2) Å and O2···Ag1 at 3.047(1) Å fall within the attractive region of Ag···O$_2$N–R interactions (Fig. S7† and also Fig. 4). Hence, the coordination geometry of Ag(I) is bent with outer sphere Ag···O contacts forming an octahedron. These results agree with the structurally related [Ag(**5NO$_2$Qu**)$_2$]X complex (X = NO_3 or ClO_4).[38,65]

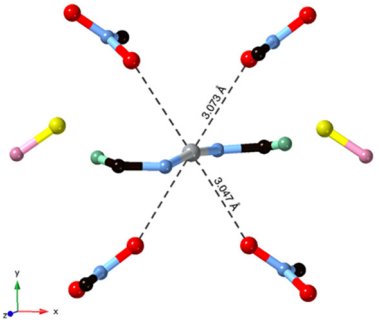

Fig. 3 The Ag interactions in [Ag(**5NO$_2$Qu**)$_2$]BF$_4$ (**1**).

It is not obvious from Fig. 2, but BF_4^- does not participate in the coordination with Ag(I) (the Ag···F1 distance is 3.856(1) Å), although it has a significant contribution to the supramolecular structure of the monomeric [Ag(**5NO$_2$Qu**)$_2$]BF$_4$ complex (Table 2). There are quite a large number of C–H···F non-covalent interactions detected which are presented in Fig. 4. The corresponding geometric parameters are depicted in Table 2. The donor–acceptor distances of the C–H···F interactions are in the range of 3.241(3)–3.470(2) Å for the C7–H7···F2 and C1–H1···F1 interactions. In addition, there are two weak C–H···O interactions between the oxygen atoms of the nitro group and the aromatic C–H groups. The donor–acceptor distances of the C3–H3···O2 and C6–H6···O1 interactions are 3.359(2) and 3.292(2) Å, respectively. A view of the packing of the monomeric complex units *via* the C–H···F and C–H···O interactions is shown in Fig. 5A.

In addition, the monomeric complex units interact with each other *via* the C···C contacts shown in Fig. 5B. The presence of a short C7···C9 contact (3.390 Å) indicated with

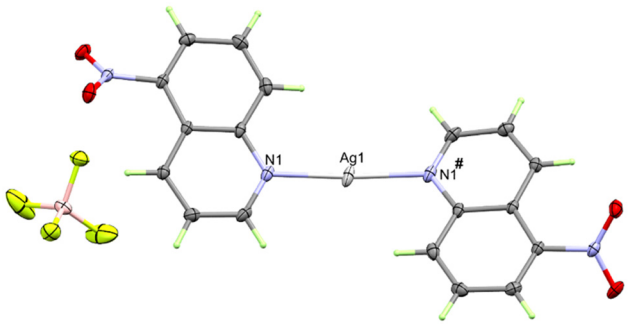

Fig. 2 The molecular structure of [Ag(**5NO$_2$Qu**)$_2$]BF$_4$ (**1**).

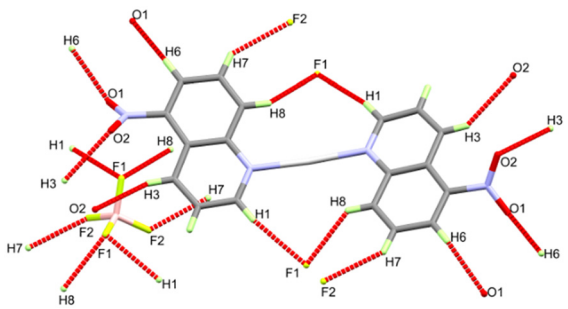

Fig. 4 All the important C–H···F and C–H···O contacts in the [Ag(**5NO$_2$Qu**)$_2$]BF$_4$ complex (**1**).

Table 2 The geometric parameters of the C–H···F and C–H···O interactions in $[Ag(5NO_2Qu)_2]BF_4$

D–H···A	D–H (Å)	H···A (Å)	D···A (Å)	D–H···A (°)	Symm. code
C1–H1···F1	0.95	2.54	3.470(2)	168	$1/2 + x, 3/2 - y, 1/2 + z$
C1–H1···F3	0.95	2.48	3.258(2)	139	$3/2 - x, 3/2 - y, 1 - z$
C3–H3···O2	0.95	2.34	2.889(1)	116	x, y, z
C3–H3···O2	0.95	2.52	3.359(2)	147	$1 - x, y, 1/2 - z$
C6–H6···O1	0.95	2.38	3.292(2)	160	$-x, y, 1/2 - z$
C6–H6···F2	0.95	2.47	2.946(1)	111	$-1/2 + x, -1/2 + y, z$
C7–H7···F3	0.95	2.44	3.157(1)	144	$1/2 - x, 3/2 - y, 1 - z$
C8–H8···F1	0.95	2.52	3.302(2)	139	$1/2 - x, 3/2 - y, 1 - z$

no doubt the presence of aromatic π–π stacking interactions with the shortest distance of 3.539(2) Å between the quinoline moieties.

3.2.2 $[Ag(Qu3CN)(H_2O)]BF_4$ (2). The structure of complex **2** is determined to have the formula $[Ag(\mathbf{Qu3CN})(H_2O)]BF_4$. It also crystallized in the monoclinic crystal system with the *C*2/*c* space group (see Table 1) and $[Ag(\mathbf{Qu3CN})(H_2O)]BF_4$ is the asymmetric formula of this polymeric structure (Fig. 6A).

It is clear from Fig. 6B that the Ag(I) is tetracoordinated with two N-atoms (N1 and N2) from two **Qu3CN** ligands. In **2**, the **Qu3CN** ligand acts as a connector between the Ag(1) sites along the *b*-direction *via* two short Ag1–N1 (2.185(4) Å) and Ag1–$N2^{\#1}$ (2.204(4) Å) bonds. In addition, the Ag(I) is coordinated with two symmetry related water molecules which also act as connectors between Ag1 sites along the *a*-direction *via* two longer Ag1–O1 (2.470(4) Å) and Ag1–$O1^{\#2}$ (2.546(4) Å) bonds. Hence, the structure of this complex could be described as a 2D polymer extended along the *ab*-plane (Fig. 7). The N(1)–Ag(1)–$N(2)^{\#1}$ and O(1)–Ag(1)–$O(1)^{\#2}$ angles are determined to be 145.81(16) and 77.11(14)°, respectively, while the N–Ag–O angles are in the range of 85.58(16)–126.40(15)° (Table 3). Hence, the AgN_2O_2 coordination sphere has a highly distorted tetracoordinated system. The distortion τ_4 parameter is estimated to be 0.62 indicating an intermediate geometry between the square planar and tetrahedral configurations.[66]

In addition, the supramolecular structure of complex **2** is controlled by the O–H···F hydrogen bonds and π–π stacking interactions presented in Fig. 8A. The 2D polymeric chains are found connected by O1–H1A···F1 and O1–H1B···F3 hydrogen bond bridges (Fig. 8B). The H1A···F1 and H1B···F3 distances are 1.86 and 2.01 Å, respectively, while the respective donor–acceptor distances are 2.693(6) and 2.802(7) Å. The O1–H1A···F1 and O1–H1B···F3 angles are 173.4 and 154.9°, respectively. In addition, the quinoline moieties are found parallel to each other leading to significant π–π interactions between the stacked aromatic systems. The C3···C7 (3.381 Å) and C5···C9 (3.348 Å) contacts are the shortest while the distance between the ring centroids is 3.658 Å.

3.3 Hirshfeld surface analysis

Hirshfeld surfaces were used to demonstrate the possible intermolecular interactions controlling the supramolecular

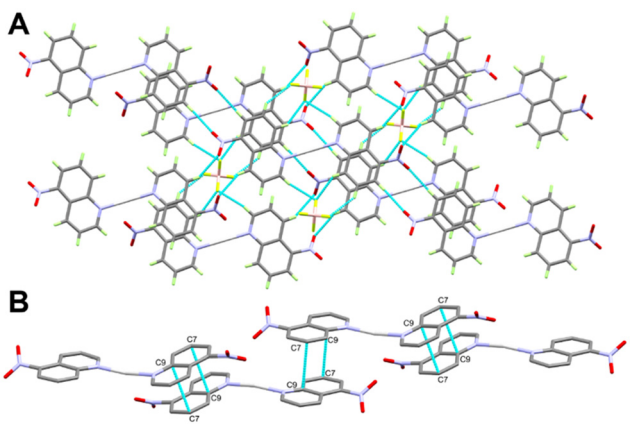

Fig. 5 Packing scheme of the $[Ag(5NO_2Qu)_2]BF_4$ complex *via* C–H···F and C–H···O contacts (A) and π–π stacking interactions (B) in the $[Ag(5NO_2Qu)_2]BF_4$ complex (**1**).

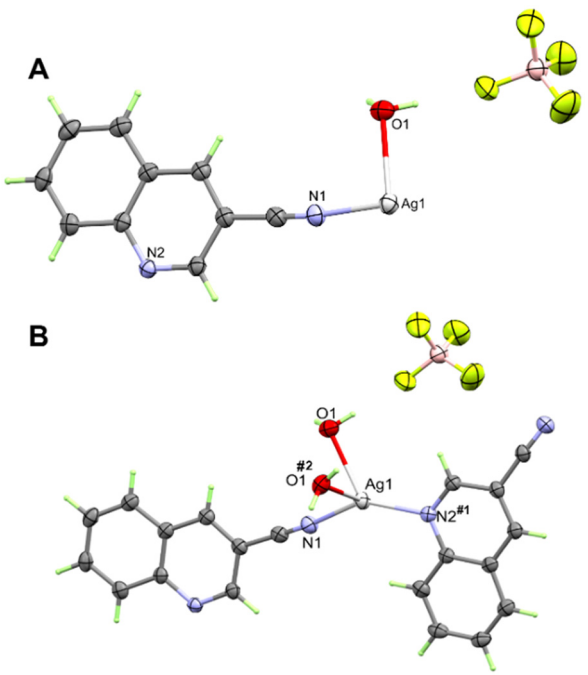

Fig. 6 Asymmetric unit (A) and coordination environment (B) of the $[Ag(\mathbf{Qu3CN})(H_2O)]BF_4$ complex (**2**). Symmetry codes for $N2^{\#1}$ and $O1^{\#2}$ are $-x + 3/2, y + 1/2$, and $-z + 3/2$ and $-x + 1, y$, and $-z + 3/2$, respectively.

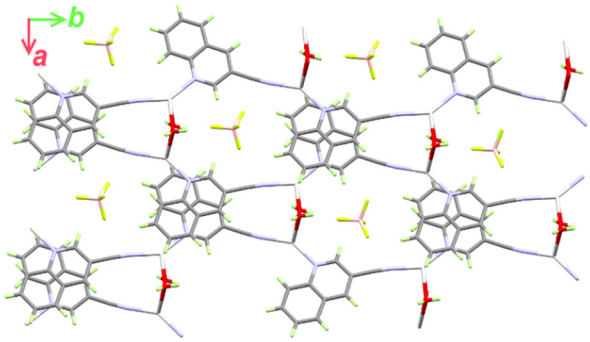

Fig. 7 Structure of the 2D polymer of complex **2**.

Table 3 Bond distances and angles (Å and °) in the [Ag(**Qu3CN**)(H_2O)]BF_4 polymer

Bond	Distance	Bond	Distance
Ag(1)–N(1)	2.185(4)	Ag(1)–O(1)	2.470(4)
Ag(1)–N(2)$^{\#1}$	2.204(4)	Ag(1)–O(1)$^{\#2}$	2.546(4)
Bonds	**Angle**	**Bonds**	**Angle**
N(1)–Ag(1)–N(2)$^{\#1}$	145.81(16)	N(1)–Ag(1)–O(1)$^{\#2}$	104.65(16)
N(1)–Ag(1)–O(1)	85.58(16)	N(2)$^{\#1}$–Ag(1)–O(1)$^{\#2}$	95.26(13)
N(2)$^{\#1}$–Ag(1)–O(1)	126.40(15)	O(1)–Ag(1)–O(1)$^{\#2}$	77.11(14)

$^{\#1}$ $-x+3/2, y+1/2, -z+3/2$ $^{\#2}$ $-x+1, y, -z+3/2$.

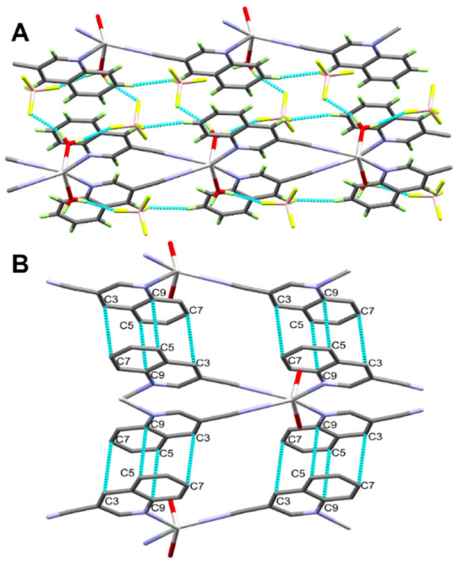

Fig. 8 Supramolecular packing structure of the 2D polymer *via* O–H···F hydrogen bonds (A) and π–π stacking (B) in complex **2**.

structure of the studied Ag(I) complexes, including hydrogen bonds, π–π stacking, C–H···π, and H···H interactions.[67,68] Also, Hirshfeld surfaces represent a 3D description of close contacts in a crystal, which are equal to or shorter than the van der Waals radii sum of interacting atoms. Also, fingerprint plots can be used to describe these contacts in a quantitative manner.[69] The Hirshfeld surfaces of complexes **1** and **2** are depicted in Fig. 9, while Fig. 10 displays the distribution selected intermolecular interactions.

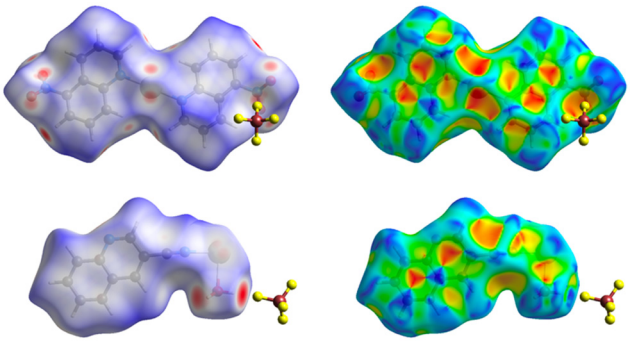

Fig. 9 Hirshfeld surfaces of complexes **1** (top) and **2** (bottom) excluding the BF_4^- counterion. From left to right mapped with the d-norm and shape index. Note that **2** is a polymer and therefore has significant spots around Ag from the propagation of the Ag–N and Ag–O bonds.

The π–π stacking is obvious for both compounds as demonstrated by the triangular pattern of the shape index. For complex **1**, the O···H (27%) and F···H (16%) contacts are the most important interactions. Additionally, there are some Ag···O (5%) interactions that contribute to the supramolecular structure. In **2**, the other most significant interaction is the F···H (27%) contact. In both complexes, all these contacts appeared as red spots in the d_{norm} map. Additionally, the dark red spots close to the Ag atom in complex **2** are related to the Ag–O and Ag–N bonds which connect the [Ag(**Qu3CN**)(H_2O)] units to form the 2D polymer.

The difference and similarities of **1** and **2** can be seen in Fig. 10 where fingerprint plots of H···F and C···C contacts can be found. The larger part played by H···F interactions in **2** is due to the hydrogen bonding of water to BF_4^-. As can be seen, the π–π stacking is similar and this is attributed to the

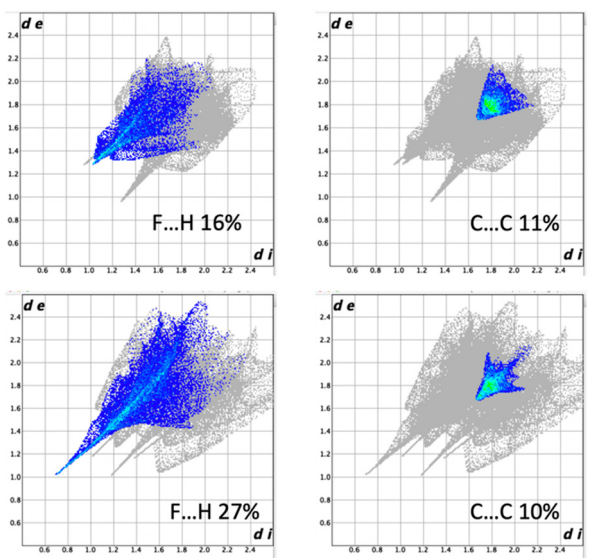

Fig. 10 The fingerprint plots of H···F and C···C contacts in complexes **1** and **2**.

Table 4 MIC and MBC of the tested compounds

Tested compound	**5NO$_2$Qu**	Complex **1**	**Qu3CN**	Complex **2**	Control
Gram positive bacteria	MIC/MBC (μg mL^{-1})				
S. aureus (ATCC 25923)	125	62.5/125	125	31.25/62.5	≤7.8[a]
MRSA (ATCC43300)	125	62.5/125	125	62.5/250	>500[a]
MRSA (1)	125	62.5/125	125	31.2/62.5	>500[a]
E. faecium (31)	125	31.2/62.5	125	62.5/125	>500[a]
Gram negative bacteria					
E. coli (ATCC 25922)	125	62.5/125	125	62.5/125	62.5[a]
K. pneumonia (ATCC 700603)	125	62.5/125	125	62.5/125	>500[a]
P. aeruginosa (ATCC 29853)	125	62.5/125	125	31.2/125	125[a]
A. baumannii (ATCC 19606)	125	31.2/62.5	125	31.2/62.5	>500[a]
P. mirabilis	125	7.8/15.6	125	15.6/62.5	125[a]
K. pneumonia (50)	125	62.5/125	125	62.5/125	>500[a]
K. pneumonia isolates (R124)	125	31.2/62.5	125	31.2/125	>500[a]
P. aeruginosa (5)	125	62.5/125	125	31.2/62.5	500[a]
A. baumannii (8)	125	31.2/62.5	500	31.2/62.5	>500[a]
Fungi					
C. albicans	125	7.8/15.6	125	31.25/62.5	15.6[b]

[a] Amoxicillin. [b] Nystatin.

relatively low coordinating ability of the BF_4^- anion, making these weaker interactions more important.

3.4 Antimicrobial studies

The results of the antimicrobial activities in terms of minimum inhibitory (MIC) and minimum bactericidal (MBC) concentrations for the tested compounds are listed in Table 4. The MIC data revealed the better antimicrobial potency of complexes **1** and **2** than the corresponding free ligands for most microbes. It is obvious that complexes **1** (MIC = 7.8 μg mL^{-1}) and **2** (MIC = 31.25 μg mL^{-1}) have higher potency against the fungus *C. albicans* than the free ligands (MIC = 125 μg mL^{-1}). It is worthy to note that the antifungal activity of **1** is considered better than that of the standard nystatin (15.6 μg mL^{-1}). The MBC results are in good agreement with this conclusion.

In terms of antibacterial activity, both Ag(I) complexes have better activities than the free ligands against all the studied bacterial strains. Complexes **1** and **2** have the best antibacterial activity against the Gram-negative bacteria *P. mirabilis*. The MIC values are determined to be 7.8 and 15.6 μg mL^{-1}, respectively, while the MBC values are 15.6 and 62.5 μg mL^{-1}, respectively. Also, both Ag(I) complexes have better activity against this microbe than the common antibiotic amoxicillin. For all Gram-negative bacteria except *E. coli* (ATCC 25922), the studied compounds have better activity than the common antibiotic amoxicillin. In addition, complex **1** (31.2 μg mL^{-1}) showed better activity against Gram positive bacteria *E. faecium* (31) than **2** (62.5 μg mL^{-1}). In contrast, complex **2** (31.2 μg mL^{-1}) has better antibacterial activity against *MRSA* (1) and *S. aureus* (ATCC 25923) than **1** (62.5 μg mL^{-1}) while both Ag(I) complexes have the same potency against *MRSA* (ATCC43300). Generally, the studied compounds have better activity against all the studied Gram-positive bacteria (except *S. aureus* (ATCC 25923)) than amoxicillin.

Neither **1** nor **2** seems to perform better than the silver nicotinate compounds we reported earlier.[70]

4. Conclusions

Single crystal X-ray diffraction was used to structurally analyze the self-assembled [Ag(**5NO$_2$Qu**)$_2$]BF_4 (**1**) and [Ag(**Qu3CN**)(H_2O)]BF_4 (**2**) complexes. Complex **1** comprised monomeric [Ag(**5NO$_2$Qu**)$_2$]BF_4 units but in contrast, complex **2** is a 2D coordination polymer *via* bridged **Qu3CN** and H_2O ligand units. Using Hirshfeld surface analysis, we show that the intermolecular interactions are significantly different in the two compounds. It is also found that complexes **1** and **2** have antimicrobial activities against several bacterial and fungal strains. Complex **1** (MIC = 7.8 μg mL^{-1}) has the best antifungal activity and is even better than the standard nystatin (15.6 μg mL^{-1}). In addition, the MIC and MBC results indicated the better antibacterial activity of **1** and **2** against *P. mirabilis* than the common antibiotic amoxicillin.

Conflicts of interest

There are no conflicts to declare.

Acknowledgements

The authors would like to extend their sincere appreciation to the Researchers Supporting Project (RSP2023R64), King Saud University, Riyadh, Saudi Arabia. FMAN and LÖ thank Chalmers University of Technology for financial support.

Notes and references

1 A. Warra, *J. Chem. Pharm. Res.*, 2011, **3**, 951–958.
2 S. Rafique, M. Idrees, A. Nasim, H. Akbar and A. Athar, *Microbiol. Mol. Biol. Rev.*, 2010, **5**, 38–45.

3 C. Biot, F. Nosten, L. Fraisse, D. Ter-Minassian, J. Khalife and D. Dive, *Parasite*, 2011, **18**, 207–214.
4 S. Monro, K. L. Colon, H. Yin, J. Roque III, P. Konda and S. Gujar, *et al.*, *Chem. Rev.*, 2018, **119**, 797–828.
5 R. G. Kenny and C. J. Marmion, *Chem. Rev.*, 2019, **119**, 1058–1137.
6 M. Claudel, J. V. Schwarte and K. M. Fromm, *Chemistry*, 2020, **2**, 849–899.
7 C. N. Morrison, K. E. Prosser, R. W. Stokes, A. Cordes, N. Metzler-Nolte and S. M. Cohen, *Chem. Sci.*, 2020, **11**, 1216–1225.
8 C. Shimokawa and S. Itoh, *Inorg. Chem.*, 2005, **44**, 3010–3012.
9 A. M. Chippindale, L. E. Head and S. J. Hibble, *Chem. Commun.*, 2008, 3010–3012.
10 Y. Wang, X. F. Wang, T. Okamura, B. Xu, W. Y. Sun and N. Ueyama, *Chin. J. Inorg. Chem.*, 2006, **22**, 1487–1490.
11 Y. H. Tan, S. P. Yang, Q. S. Li and Y. L. Tan, *Chin. J. Struct. Chem.*, 2006, **25**, 1387–1391.
12 S. V. Ivanov, S. M. Miller, O. P. Anderson and S. H. Strauss, *Cryst. Growth Des.*, 2004, **4**, 249–254.
13 A. V. Artem'ev, A. Y. Baranov and I. Y. Bagryanskaya, *Inorg. Chem. Commun.*, 2022, **140**, 109478.
14 H. Wu, S. O. Aderinto, Y. Xu, H. Zhang and Z. Yang, *J. Chem. Res.*, 2016, **40**, 492–497.
15 G. Kleinhans, A. K. W. Chan, M. Y. Leung, D. C. Liles, M. A. Fernandes and V. W. W. Yam, *et al.*, *Chem. – Eur. J.*, 2020, **26**, 6993–6998.
16 H. Lang, M. Leschke, G. Rheinwald and M. Melter, *Inorg. Chem. Commun.*, 1998, **1**, 254–256.
17 A. G. Young and L. R. Hanton, *Coord. Chem. Rev.*, 2008, **252**, 1346–1386.
18 F. Pointillart, P. Herson, K. Boubekeur and C. Train, *Inorg. Chim. Acta*, 2008, **361**, 373–379.
19 M. Osawa and M. Hoshino, *Chem. Commun.*, 2008, 6384–6386.
20 C.-Y. Wu, C.-S. Lee, S. Pal and W.-S. Hwang, *Polyhedron*, 2008, **27**, 2681–2687.
21 H.-T. Shi, T. Duan, C. Xu and Q.-F. Zhang, *Z. Naturforsch., B: J. Chem. Sci.*, 2009, **64**, 204–208.
22 C. Liu, P.-K. Liao, C.-S. Fang, J.-Y. Saillard, S. Kahlal and J.-C. Wang, *Chem. Commun.*, 2011, **47**, 5831–5833.
23 E. J. Fernández, A. Laguna, J. M. López-de-Luzuriaga, M. Monge, M. Montiel and M. E. Olmos, *et al.*, *Dalton Trans.*, 2005, 1162–1164.
24 P. J. Malinowski, D. Kurzydłowski and W. Grochala, *Dalton Trans.*, 2015, **44**, 19478–19486.
25 H. Yang, J. Lei, B. Wu, Y. Wang, M. Zhou and A. Xia, *et al.*, *Chem. Commun.*, 2013, **49**, 300–302.
26 Q.-H. Wei, L.-Y. Zhang, L.-X. Shi and Z.-N. Chen, *Inorg. Chem. Commun.*, 2004, **7**, 286–288.
27 Q. L. Ni, F. Zhang, T. H. Huang, X. P. Wu, X. J. Wang and G. M. Liang, *et al.*, *Z. Anorg. Allg. Chem.*, 2015, **641**, 2664–2669.
28 A. A. Adeleke, S. J. Zamisa, M. S. Islam, K. Olofinsan, V. F. Salau and C. Mocktar, *et al.*, *Molecules*, 2021, **26**, 1205.
29 M. S. Altowyan, M. A. El-Naggar, M. A. Abu-Youssef, S. M. Soliman, M. Haukka and A. Barakat, *et al.*, *Crystals*, 2022, **12**, 356.
30 M. A. El-Naggar, M. A. Abu-Youssef, S. M. Soliman, M. Haukka, A. M. Al-Majid and A. Barakat, *et al.*, *J. Mol. Struct.*, 2022, **1264**, 133210.
31 M. Cavicchioli, A. C. Massabni, T. A. Heinrich, C. M. Costa-Neto, E. P. Abrão and B. A. Fonseca, *et al.*, *J. Inorg. Biochem.*, 2010, **104**, 533–540.
32 M. Kaloğlu, N. Kaloğlu, S. Günal and İ. Özdemir, *J. Coord. Chem.*, 2022, **74**, 3031–3047.
33 S. Medici, M. Peana, V. M. Nurchi and M. A. Zoroddu, *J. Med. Chem.*, 2019, **62**, 5923–5943.
34 J.-Y. Maillard and P. Hartemann, *Crit. Rev. Microbiol.*, 2013, **39**, 373–383.
35 S. Medici, M. Peana, G. Crisponi, V. M. Nurchi, J. I. Lachowicz and M. Remelli, *et al.*, *Coord. Chem. Rev.*, 2016, **327**, 349–359.
36 R. I. Khusnutdinov, A. R. Bayguzina and U. M. Dzhemilev, *J. Organomet. Chem.*, 2014, **768**, 75–114.
37 S. Yamashkin and E. Oreshkina, *Chem. Heterocycl. Compd.*, 2006, **42**, 701–718.
38 A. A. Massoud, V. Langer, Y. M. Gohar, M. A. Abu-Youssef, J. Jänis and G. Lindberg, *et al.*, *Inorg. Chem.*, 2013, **52**, 4046–4060.
39 A. Garrido Montalban, in *Quinolines and Isoquinolines*, ed. K. C. Majumdar and S. K. Chattopadhyay, Wiley-VCH Verlag GmbH & Co. KGaA, Germany, 2011, pp. 299–339.
40 V. V. Kouznetsov, C. M. M. Gómez, J. L. V. Peña and L. Y. Vargas-Méndez, in Natural and synthetic quinoline molecules against tropical parasitic pathologies: An analysis of activity and structural evolution for developing new quinoline-based antiprotozoal agents, *Discovery and Development of Therapeutics from Natural Products Against Neglected Tropical Diseases*, Elsevier, 2019, pp. 87–164.
41 Y. B. Rajesh, in *Quinoline heterocycles: synthesis and bioactivity*, ed. B. P. Nandeshwarappa and S. O. Sadashiv, 2018.
42 P. M. O'Neill, R. C. Storr and B. K. Park, *Tetrahedron*, 1998, **54**, 4615–4622.
43 J. Casal and S. Asís, *Austin Tuberculosis: Research & Treatment*, 2017, **2**, 1007–1010.
44 S. Kumar, S. Bawa and H. Gupta, *Mini-Rev. Med. Chem.*, 2009, **9**, 1648–1654.
45 S. Adsule, V. Barve, D. Chen, F. Ahmed, Q. P. Dou and S. Padhye, *et al.*, *J. Med. Chem.*, 2006, **49**, 7242–7246.
46 H. Beyzaei, H. H. Moghadam, G. Bagherzade, R. Aryan and M. Moghaddam-Manesh, *Avicenna J. Med. Biochem.*, 2019, **7**, 9–15.
47 S. A. Khan, A. M. Asiri, S. H. Al-Thaqafy, H. M. Faidallah and S. A. El-Daly, *Spectrochim. Acta, Part A*, 2014, **133**, 141–148.
48 V. Arjunan, P. Ravindran, T. Rani and S. Mohan, *J. Mol. Struct.*, 2011, **988**, 91–101.
49 P. Smoleński, S. W. Jaros, C. Pettinari, G. Lupidi, L. Quassinti and M. Bramucci, *et al.*, *Dalton Trans.*, 2013, **42**, 6572–6581.

50 T. P. Andrejević, I. Aleksic, J. Kljun, M. Počkaj, M. Zlatar and S. Vojnovic, *et al.*, *RSC Adv.*, 2023, **13**, 4376–4393.
51 J. K. Aulakh, T. S. Lobana, H. Sood, D. S. Arora, R. Kaur and J. Singh, *et al.*, *RSC Adv.*, 2019, **9**, 15470–15487.
52 M. A. El-Naggar, J. H. Albering, A. Barakat, M. A. Abu-Youssef, S. M. Soliman and A. M. Badr, *Inorg. Chim. Acta*, 2022, **537**, 120948.
53 G. M. Sheldrick, *Program for empirical absorption correction of area detector data, Sadabs*, 1996.
54 (*a*) A. S. Bruker, Bruker A. Inc., Madison, Wisconsin, USA, 2004; (*b*) G. M. Sheldrick, *Acta Crystallogr., Sect. A: Found. Crystallogr.*, 1990, **46**, 467–473.
55 F. L. Hirshfeld, *Theor. Chim. Acta*, 1977, **44**, 129–138.
56 M. Turner, J. McKinnon, S. Wolff, D. Grimwood, P. Spackman and D. Jayatilaka, *et al.*, *CrystalExplorer17*, University of Western Australia, 2017, **https://crystalexplorer.net/download/**.
57 P. Wayne, Clinical and Laboratory Standards Institute: Performance standards for antimicrobial susceptibility testing: 20th informational supplement, CLSI document M100-S20, 2010.
58 R. W. Beal and T. B. Brill, *Appl. Spectrosc.*, 2005, **59**, 1194–1202.
59 A. N. Khlobystov, A. J. Blake, N. R. Champness, D. A. Lemenovskii, A. G. Majouga and N. V. Zyk, *et al.*, *Coord. Chem. Rev.*, 2001, **222**, 155–192.
60 A. M. Alshima'a, Y. M. Gohar, V. Langer, P. Lincoln, F. R. Svensson and J. Jänis, *et al.*, *New J. Chem.*, 2011, **35**, 640–648.
61 K. Nomiya, K. Tsuda, T. Sudoh and M. Oda, *J. Inorg. Biochem.*, 1997, **68**, 39–44.
62 K. Nomiya, R. Noguchi and M. Oda, *Inorg. Chim. Acta*, 2000, **298**, 24–32.
63 S. Nawaz, A. A. Isab, K. Merz, V. Vasylyeva, N. Metzler-Nolte and M. Saleem, *et al.*, *Polyhedron*, 2011, **30**, 1502–1506.
64 A. A. Isab, S. Nawaz, M. Saleem, M. Altaf, M. Monim-ul-Mehboob and S. Ahmad, *et al.*, *Polyhedron*, 2010, **29**, 1251–1256.
65 M. S. Altowyan, N. H. Al-Shaalan, A. A. Alkharboush, A. Barakat and S. M. Soliman, *Symmetry*, 2022, **14**, 547.
66 L. Yang, D. R. Powell and R. P. Houser, *Dalton Trans.*, 2007, 955–964.
67 H. F. Clausen, M. S. Chevallier, M. A. Spackman and B. B. Iversen, *New J. Chem.*, 2010, **34**, 193–199.
68 M. A. Spackman and D. Jayatilaka, *CrystEngComm*, 2009, **11**, 19–32.
69 M. A. Spackman and J. J. McKinnon, *CrystEngComm*, 2002, **4**, 378–392.
70 M. A. Abu-Youssef, R. Dey, Y. Gohar, A. A. Massoud, L. Öhrström and V. Langer, *Inorg. Chem.*, 2007, **46**, 5893–5903.